Lawrence Berkeley National Laboratory
Recent Work

Title
Calculations of carrier localization in In/sub x/Ga/sub 1-x/N

Permalink
https://escholarship.org/uc/item/73c7m09c

Journal
Physical Review B, 63(24)

Author
Wang, Lin-Wang

Publication Date
2001-04-04

eScholarship.org Powered by the California Digital Library
University of California

Calculations of Carrier Localization in InGaN

Lin-Wang Wang

NERSC, Lawrence Berkeley National Laboratory, Berkeley, CA 94720

Abstract

The electronic structures of cubic InGaN systems are calculated using an atomistic empirical pseudopotential method. Two extreme cases are studied. One is a pure InN quantum dot embedded in a pure GaN matrix, another is a pure $In_xGa_{1-x}N$ alloy without clustering. We find hole localizations in both cases. The hole wavefunction starts to be localized as soon as a few In atoms segregate to form a small cluster, while the electron wavefunction only becomes localized after the number of In atoms in the quantum dot becomes larger than 200. The hole state is also strongly localized in a pure $In_xGa_{1-x}N$ alloy, on top of randomly formed (110) directioned In-N-In chains. Using one proposed model, we have calculated the hole energy fluctuation, and related that to photoluminescence line width. The calculated line width is around 100 meV, close to the experimental results. Wurtzite InGaN is also studied for optical anisotropies. We find that in both quantum dot and pure alloy, the polarization is in the xy-plane perpendicular to the c-axis of the wurtzite structure.

PACS numbers: 71.15.Hx, 71.20.Nr, 78.20.-e

I. INTRODUCTION

The success of blue color lasing using InGaN as the active material[1–3] has inspired a tremendous amount of recent research in this material. The coexistence of the high quantum yield of the photoluminescence (PL) and the high density of the threading dislocation[4] indicates strong carrier localization. This means that an exciton is localized in space before it can reach the impurity sites to be annihilated nonradiatively. One current focus of research is to understand the mechanism of this localization. One possibility is the formation of InN quantum dots in the InGaN alloy[5–8]. Another possibility is the localization caused by natural composition fluctuations in pure InGaN, without clustering and the formation of quantum dots[9,10].

Although there are mounting experimental reports about the inhomogeneity of the In composition in GaInN, an exclusive evidence for the formation of nanometer InN quantum dot is yet to come. A spatially resolved Cathodoluminescence spectra[11] shows the PL from localized spots, but the resolution is too gross to resolve fine structures in nanometer scale. Atomic Force microscope (AFM) images[11] also show grooves in an uncapped InGaN sample. But it is not clear how that is related to possible In concentration fluctuation. Recent resonant Raman scattering experiments[12,13] show that the In concentration in the area of wavefunction localization is around 80%, much larger than its nominal concentrations in the samples studied. However, as we will point out later, this could be true even in pure InGaN alloy. A more direct measurement comes from the cross section image of transmission electron microscopy (TEM)[14]. It does show some nanometer scale dot like structures in the InGaN multiple quantum well, and large local In concentration fluctuations in such systems. However, caution must be taken, since a TEM image represents a projection sum of the charge density, and is affected more by strain than the chemical identities of the atoms. One often cited reason for In segregation is the spinodal instability of $In_xGa_{1-x}N$ alloy for the x range of the samples studied here. This is concluded from valence force field (VFF) calculations[15] of the atomistic strain in the alloy. The separation of the In rich

part and the In poor part is to release the strain. However, this is only true for incoherent separation of these two parts. If the system is still coherent, the formation of the quantum dot will only increase the strain energy, rather than decrease it. This is shown in our own VFF calculations. So, the spinodal instability is only true for incoherent formation of the quantum dot, not for coherent formation. For nanometer quantum dot, if each quantum dot is incoherent to its matrix, there might be too much surface (or dislocation) energy to justify the gain due to the release of strain energy. Thus, unless the dislocation energy and the growth kinetics are studied carefully, one cannot simply conclude that the quantum dot must be formed thermodynamically due to the spinodal instability. A recent refine calculation[16] showed that the surface solubility of In in GaN (which is relevant for vapor-phase growth) is much higher than the bulk solubility. As a result, in low In concentration, clustering of In is not expected in vapor-phase grown samples.

Given the current experimental uncertainties about the quantum dot formation and its profile in InGaN, it is useful to theoretically investigate the electronic states of the system in different scenarios. Here we will study two extreme cases at the two ends of the spectrum. One is a pure InN quantum dot embedded in GaN matrix. Here the variable is the diameter D of the quantum dot. Another case is a pure $In_xGa_{1-x}N$ alloy, without any clustering (or say short and long range ordering). The variable here is the In composition x. We will study, in each case, how strong is the carrier localization, and what the wavefunction looks like. We will study them as functions of the variable D and x.

II. METHODS

We will use empirical pseudopotential calculations to study these systems. The empirical pseudopotential method (EPM) has been used to study InGaN and InGaAsN system[17,18] previously. Its reliability and applicability to such systems have been investigated before. However, previous studies either focused on the As rich side of the InGaAsN quanternary system[17], where the property is dominated by the impurity N, or on a single In impurity[18] in GaN. No systematic study has been carried out to address the carrier localization issue

in the InGaN system. Here, we will use exactly the same EPM as in the previous work[18] to study the carrier localization.

In the empirical pseudopotential method, the total potential of the system is constructed nonselfconsistently from screened individual atomic potentials v_α. This leads to a single particle Hamiltonian:

$$\Big[-\frac{1}{2}\nabla^2 + \sum_{\alpha,\mathbf{R}_\alpha} v_\alpha(\mathbf{r}-\mathbf{R}_\alpha;\epsilon_{ij})\Big]\psi_i(\mathbf{r}) = \epsilon_i\psi_i(\mathbf{r}), \qquad (1)$$

where $\{\mathbf{R}_\alpha\}$ are the atomic positions of atom species α. The screened atomic potentials v_α are fitted to experimental and first principle calculated band structures, band off-sets, effective masses and deformation potentials. They explicitly depend on the local atomic strains ϵ_{ij} in order to mimic the charge density self-consistency. The wavefunction $\psi_i(\mathbf{r})$ is expanded in a plane wave basis with an energy cutoff of 7.7 Ryd. In this work, we have used exactly the same screened atomic pseudopotentials v_α as given in Ref. 18. Unlike other empirical pseudopotentials, for which different N atomic potentials are used in InN and GaN, the current EPM has the same N potential for both InN and GaN. This enhances the reliability of the EPM in this system. The Schrodinger's equation (1) is solved using the folded spectrum method[19] for the valence band maximum (VBM) and conduction band minimum (CBM) states for periodic systems containing thousands of atoms. The calculations are carried out on NERSC's Cray T3E parallel computer via a program called Escan[20].

III. InN QUANTUM DOT IMBEDDED IN GaN MATRIX

We first study zincblende InGaN systems. The spin-orbit splitting is only about 10 meV in the cubic system[21], thus we have neglected it in our calculation. We first study the case of an InN quantum dot embedded in a GaN matrix. The effects of a single In atom has been studied in Ref. 18. It was found that a single In atom will induce a resonant VBM state. This resonant state has a strong wave function peak at the In atom, but is not energetically bound (thus localized). Starting with this single In atom, we add more In atoms to form

In clusters (quantum dots). More specifically, in a GaN crystal, within a sphere of radius R centered at one cation site, we have changed the Ga atoms to In atoms. We have created 6 quantum dots in this way, with their numbers of In atoms being: 1,13,43,201,627,1433. For the 13 In atom case, it corresponds to one central In atom and 12 fcc first nearest neighbors. The diameters of these six quantum dots are 3.5, 8.3, 12.4, 20.8, 30.4, 40.0 $\AA$ respectively. To embed these InN quantum dots in GaN matrix, for the first three quantum dots, we have used a supercell of 4096 atoms ($4a \times 4a \times 4a$, where a is the lattice constant), while a 32768 atom supercell ($8a \times 8a \times 8a$) is used for the last three quantum dots. The valence force field (VFF)[22] method is used to relax the internal atomic positions. The same VFF parameters used in Ref. 18 are used here.

The calculated hole and electron wavefunctions are shown in Fig.1 and their energies are plotted in Fig.2. From the calculation, we have the following observations: (1) The hole wavefunction is localized starting from the 13 In cluster. (2) The electron wavefunction is not localized until (after) the 201 In atom cluster. But, here we have not considered the Coulomb interaction between electron and hole. The electron wavefunction can be bound to the hole by forming an exciton. Thus, even in the 13 In atom case, the exciton can be localized through the localization of the hole. There are three bound electron states in the 1433 In atom quantum dot. (3) In the large quantum dots (e.g, 627 and 1433 In atoms), the hole wavefunctions are localized around the (110) corners of the quantum dot (although the quantum dot itself is spherical). The same phenomena has been observed previously in InP quantum dots embedded in GaP[23]. (4) The hole binding energy, as shown in Fig.2, saturates quickly around 600 meV after the number of In atoms becomes larger than 43.

In summary, a small segregation of In atoms will be enough to localize the hole wavefunction in a pure GaN matrix.

IV. PURE InGaN ALLOY

We next study the case of pure $In_xGa_{1-x}N$ zincblende alloy. In this case, In atoms are randomly distributed at the zincblende cation sites. No short and long range orders exist

in such a system. Again, the internal atomic positions are relaxed using the VFF model, and the wavefunctions in Eq(1) are solved using the folded spectrum method. The question here is: is there a carrier localization in such a system? Fig.2 shows a VBM wavefunction in a 32768 atom supercell of $In_{0.2}Ga_{0.8}N$. The VBM wavefunction is localized in a slim cylinder shape about 15 $\AA$ long, while the CBM wavefunction (which is not shown here) is extended uniformly. Upon a closer inspection, we found that the VBM localization site corresponds to a single chain of In atoms (or say an In-N-In chain). This chain is formed by chance, and in a large enough supercell, such a chain will always exist. Many random configurations of $In_xGa_{1-x}N$ alloy were calculated, and we always found the VBM localized on top of such In atom chains. Logarithmic projection views along and perpendicular to the cylinder axis are also shown in Fig.3(b) and (c) respectively. They reveal a decay length λ of 3.8 $\AA$ in an $exp(-x/\lambda)$ description of the ψ^2 tail. This VBM state should be the localized tail states in the density of state (DOS) of a random system, as described by Anderson's, and Lifshits's theories[24,25]. The difference between this system and a more conventional system like GaAlAs is the size of the localization. In the $Ga_{0.4}Al_{0.6}As$ alloy, the VBM state is localized in a region which encompasses more than 20,000 atoms[26], while here, the number of In atoms related to the localization is around 5-7. Due to this strong localization, the cause of the localization is better described by the random formation of the In-N-In chains, rather than composition fluctuation in one area. Thus, the characterization of the carrier localization in this system is different from the conventional alloy. This will lead to different results (e.g, the trend of PL linewidth with x) from the conventional alloys. Notice that, the eigen energy of the VBM state in Fig.3 is -7.285, which is higher than some of the eigen energies in Fig.2, which are -7.812, -7.467, -7.364, -7.322, -7.271, -7.223, respectively from the small to the large quantum dots. This means, if $In_{0.2}Ga_{0.8}N$ was the barrier instead of pure GaN, the smallest four quantum dots in Fig.1 would not have bound hole states inside the dot.

One important quantity to be calculated is the photoluminescence (PL) line width. To calculate this quantity, let's first propose a model of the carrier dynamics in the PL process.

In this model, the electron and hole pair is optically excited randomly at one position. Then the hole will diffuse to a nearby localized state, and stay there. The electron will be attracted to the hole by the Coulomb interaction, and they form an exciton. The radiative emission will come from this localized exciton. The localization and the energy fluctuation are due to the hole state. The diffusing distance of the hole should be smaller than the average impurity-impurity distance, so the exciton will not be annihilated nonradiatively by impurities.

Guided by this model, we propose here a method to calculate the energy fluctuation. We first take a $L \times L \times L$ supercell. We then assign the N_c cation sites in the supercell to In and Ga atoms according to x and 1-x probabilities. For each alloy configuration, the number of In atom N_{In} in the system may be different from the nominal xN_c. This leads to an actual composition $x' = N_{In}/N_c$ for this particular configuration. As a result, the length of the supercell size L is adjusted accordingly[27]. After the VFF atomic position relaxation, the calculated VBM state in this supercell will be the final hole state of one photoluminescence event. By repeating the calculation with different alloy configurations, we will have the random fluctuation of the PL energy.

One uncertainty of this approach is the size L of the supercell. The volume of the supercell represents the area that the hole explored for higher energy states before its radiative decay. One can use the average diffusion length D_h of the hole for L. But that will probably over estimate the supercell volume, since not all the areas in $D_h \times D_h \times D_h$ might have been effectively explored by the hole. The second way of estimating L is the following. For the hole to stay in its final localized state a_1, its hopping time t to another higher energy state a_2 should be longer than its radiative decay time τ. In our supercell calculation, the a_1 is the VBM inside the supercell, and a_2 could be a state in an adjacent supercell. Thus, on average, the $a_1 - a_2$ distance is L. Then the overlap $|<a_1|a_2>|^2$ should be $exp(-L/\lambda)$, where λ is the decay length of the localized state (3.8 $\mathring{A}$ as shown in Fig.3). If we assume the hopping time is t_0 if a_1 and a_2 are spatially on top of each other, then $t = t_0 exp(L/\lambda)$. On the other hand, if a_0 is the Bohr radius of the electron wavefunction bound to the localized hole,

then the optical oscillator strength should be $P_0\Omega/(4\pi a_0^3/3)$, where Ω is the hole localization volume and P_0 is the oscillator strength when there is a full overlap between electron and hole. Thus, $\tau = \tau_0(4\pi a_0^3/3)/\Omega$, and τ_0 is the radiative life time corresponding to P_0. Then finally, $t \sim \tau$ can be used to estimate L. This leads to: $L = \lambda ln((\tau_0(4\pi/3)a_0^3/t_0\Omega)$. One uncertainty in this formula is t_0. But fortunately, the final result of L is not very sensitive to its exact value. We can use $t_0 = 1ps$, as estimated from phonon cooling in a semiconductor quantum dot[28]. The other parameters can be obtained as: $\tau_0 \sim 100$ ps, as measured from the time dependent PL signal in pure GaN[29]; $a_0 \sim 25\AA$, as calculated by ϵ/m_e, where ϵ is the dielectric constant, and m_e is the electron effective mass; and $\Omega = 100\AA^3$, as estimated from Fig.3. Then, we have $L \sim 40\AA$.

The above value of L is just an estimate. Here we have first calculated the hole state fluctuations using a supercell of 512 atoms. This corresponds to an L ($= 4a$, a is the lattice constant) of $\sim 20\AA$, about the same size as the localization length, and is probably at the lower end of the plausible range of L. Later, we will discuss the dependences of our results on L. We have calculated five x compositions. For each composition, we calculated 40 atomic configurations. The energy fluctuations are shown in Fig.4 for the $In_{0.2}Ga_{0.8}N$ alloy. In Fig.4(a), the CBM energy of the supercell is plotted against the total number of In atoms randomly generated in the supercell. The relationship is almost linear. This is because the CBM is a conventional uniformly extended state. As a result, its energy is dictated by the average band edge potential, thus the total number of In atoms in the supercell. Notice that, in reality, the size of the electron wavefunction is determined by the Bohr radius a_0 of the hydrogen state bound to the hole, which is much larger than the 512 atom supercell. As a result, its energy fluctuation is much smaller than what is shown in Fig.4(a) and its contribution in the PL energy fluctuation can be ignored.

Figure 4.(b) shows the big fluctuations of the hole state energy, corroborating the strong spatial localization. The eigen energy has almost no correlation to the number of In atoms in the supercell. The full width of the half maximum (FWHM) (ΔE) of the PL peak can be calculated from the standard deviation of the hole state energy in Fig.4(b), and a Gaussian

model for the PL peak profile. The resulting ΔE for different compositions are shown in Fig.5(a). The PL line width is around 100 meV and it decreases with increasing x. This value of ΔE is about 100 times larger than that of a conventional alloy, like $GaInAs$[30]. This is another manifestation of the strong hole localization. To investigate the supercell size L dependence of ΔE, we have also calculated ΔE of $In_{0.2}Ga_{0.8}N$ using $L = 8a$ (4096 atom supercell), and $L = 16a$ (32768 atom supercell), where a is the lattice constant. We calculated 40 alloy configurations for $L = 8a$, but only 20 configurations for $L = 16a$ due to computer resource constraints. The resulting ΔE for $L = 4a, 8a, 16a$ are 87, 69, and 72 meVs respectively. We see a slight decrease of ΔE when L increases, and a possible jitter from $L = 8a$ to $L = 16a$ due to the small numbers of configurations used, but the change of ΔE is relatively small. The ΔE decreases by a factor of 1.2 from $L = 4a$ to $L = 16a$, although the volume has been increased 64 times. According to our model estimations above, the correct L should fall into the range of the L's we have tested here (from 18$\AA$ to 74$\AA$). This gives us some confidence that the ΔE in Fig.5(a) should be correct (perhaps within a factor of 1.5 for the uncertainties of L).

The ΔE in Fig.5(a) is close to the experimental values at low temperature (see Ref. 32 or the values cited in Ref. 33). But one big difference is the trend of ΔE with x. While our result shows a decrease of ΔE with increasing x, the experimental result[32] shows an increase of ΔE. In conventional alloys (e.g., $GaAlAs$), the eigen energy fluctuation is proportional to the fluctuation of the total number of a given atomic species within the exciton volume[31]. Thus, the larger the x (up to 0.5), the bigger the fluctuation. In our strongly localized system, the energy fluctuation depends on the fluctuation of forming the small In atomic chains. the smaller the x, the larger is the fluctuation of forming such small chains, thus larger is the eigen energy fluctuation as shown in Fig.5(a). The reason why the experimental ΔE increases with increasing x is not clear at this stage. Although in the same trend, the experimental $\Delta E(x)$ does not fit well[32] to the formula of conventional alloys either. One explanation is that the experimental sample is not homogeneous as suggested by many recent experiments discussed in the introduction, and the inhomogeneity increases with increasing

x. This leads to an increasing ΔE with x. This effect has been discussed in Ref. 33.

In Fig.5(b), we plotted the average VBM energy E^{ave}_{VBM} as a function of x. As shown previously in Ref. 18, there is a maximum of E^{ave}_{VBM} around $x = 0.3$. Notice that the average E^{ave}_{VBM} also depends on the supercell size L. For $L = 4a, 8a$, and $16a$, we have $E^{ave}_{VBM} = -7.394, -7.327$, and -7.274 eV respectively for the $In_{0.2}Ga_{0.8}N$ alloy. The increase in E^{ave}_{VBM} has a similar magnitude to the energy fluctuation ΔE. In Fig.5(c) we plotted the average band gap E_{gap} as a function of x, and compared that with the experimentally measured results. The dashed line in Fig.5(c) is a linear fit to the PL data in Ref. 32, and it has been shifted downward by 0.1 eV to compensate for the fact that the experimental sample is in a wurtzite structure and is measured at room temperature. The overall slope of the experimental PL energy in the range of $0 < x < 0.15$ agrees well with our calculated results.

Finally, to relate to the Raman experiments[12,13] where the In concentrations on top of the carrier wavefunctions are measured, we have tried to estimate this quantity and have plotted the result in Fig.5(d). What is shown in Fig.5(d) is the following. Suppose $\{\mathbf{R}_{In}\}$ are the In atomic positions, and $\{\mathbf{R}\}$ are the atomic positions for both In and Ga atoms. Then the In percentage in the VBM wavefunction $\psi_{VBM}(r)$ [plotted in Fig.5(d)] is calculated as: $\int[\sum_{R_{In}} exp(-(r-R_{In})^2/w^2)]\psi_{VBM}(r)^2 d^3r / \int[\sum_{R} exp(-(r-R_{In})^2/w^2)]\psi_{VBM}(r)^2 d^3r$, here w is a Gaussian width, and we have used $w = 0.53\mathring{A}$. Measured by this formula, the In concentration around the wavefunction is significantly larger than the nominal x. Thus, one cannot use the high In concentration from Raman data to conclude that the PL emission must come from a quantum dot.

V. WURTZITE InGaN SYSTEMS

In this final section, we would like to investigate the wurtzite structure. Although zincblende InGaN can be grown on cubic substrate, like (100) GaAs[34], most InGaN experiments are done in the wurtzite structure. The purpose here is to find whether there is any optical anisotropy between the wurtzite c-direction and the perpendicular xy direc-

tions. We have used the same empirical pseudopotentials to calculate the wurtzite InGaN. However, to get appropriate bulk GaN and InN crystal field splitting, we did not use the ideal wurtzite crystal structure. Instead, in the VFF calculation, we have slightly modified the ideal bond angle for those bond angles consisting of one c-axis bond. The ideal angle changes from 109.47 to 108.73 and 107.32 for GaN and InN respectively. The unit cell and the internal atomic positions are relaxed using the resulting VFF model, and the resulting crystal field splittings are 19 meV and 13 meV for GaN and InN respectively, consistent with the available experimental data[21]. Spin-orbit interaction is also introduced through a nonlocal pseudopotential, and a doubling of the wavefunction to spin up and spin down components[35]. Fitting to the experimental results[21], we have used 10.3 meV and 10.9 meV spin-orbit splittings for GaN and InN respectively.

We have calculated two quantum dots, with 209 and 641 In atoms respectively. The band gaps (without the Coulomb energy between the electron and hole) for these two quantum dots are 2.959 and 2.634 eV respectively. They are slightly larger than the corresponding zincblende results of 2.770 and 2.547 eV for zincblende quantum dots with 201 and 627 In atoms. This is mainly because our EPM InN wurtzite band gap of 2.035 eV is larger than the zincblende counter part of 1.784 eV. The important fact is that, for both wurtzite quantum dots, the optical transitions from CBM to the top valence band states (within 30 meV of the VBM), are all polarized in the xy directions.

We next performed a wurtzite $In_{0.2}Ga_{0.8}N$ alloy calculation. A 572 atom supercell was used, and 40 atomic configurations were calculated. The corresponding ΔE is 93 meV, this is very close to the 87 meV result of zincblende $In_{0.2}Ga_{0.8}N$. 70% of the VBM states are localized in the xy plane, along randomly formed In-N-In chains. The other 30% are localized along an inclined direction close to the c direction (we will call it z direction localization), with on average lower VBM energies. When larger supercells are used, more of the VBM states are found in the xy plane. The averaged VBM energy of the 572 atom supercell is -7.438 eV, which is close to the corresponding zincblende result of -7.394 eV for the 512 atom supercell. The In concentration of the VBM in wurtzite $In_{0.2}Ga_{0.8}N$ is also close to

the zincblende result of Fig.5(d). We found that, in the wurtzite structure, besides the single In-N-In chain localizations, there are also cases of double stacked xy-plane localizations and more complicated localization shapes. As for the polarization, if the hole wavefunction is localized in the xy directions, then the transition is polarized in the xy plane, otherwise, it is polarized along the z(c) direction. Since there are more xy localization than the z localization, and since on average, the z direction localized states have lower valence state energy, the experimentally observed PL should be mostly xy direction polarized. Thus, the polarization in the alloy is similar to that in a quantum dot. Unfortunately, one cannot use optical polarization to distinguish the case of a pure alloy from that of quantum dots.

VI. CONCLUSIONS

We have investigated carrier localization in InGaN system using the empirical pseudopotential method. We have studied two extreme cases: a pure InN quantum dot embedded in a pure GaN matrix and $In_xGa_{1-x}N$ without clustering. We found the following: (1) For InN quantum dot, the hole state starts to be localized after a few In atoms segregate to form a quantum dot, but the electron state is localized only after there are more than 200 In atoms in the quantum dot. (2) The hole binding energy does not change much after the quantum dot diameter is larger than 15 $\AA$. (3) In a pure $In_xGa_{1-x}N$ zincblende alloy, the hole wavefunctions are localized strongly on randomly formed short (110) $In-N-In$ chains, while the electron wavefunctions are extended uniformly. The exponential decay length of the hole state is about 3.8 $\AA$. (4) Large hole energy fluctuations exist, which correspond to a $\sim$ 100 meV linewidth ΔE of the photoluminescence. This is about 100 times larger than that in a conventional alloy like GaInAs. (5) Due to the strong hole localization, the trend of $\Delta E(x)$ with x is different from that of the conventional alloy due to composition fluctuation. Currently, our calculated $\Delta E(x)$ has a different trend than the experimental result, although the magnitudes of them are similar. This might be due to inhomogeneities of the experimental alloy samples. (6) In an alloy, the In concentration on top of the hole wavefunction is significantly larger than the nominal In concentration x. Thus, one cannot

use the high In concentration from the Raman scattering data to conclude that the PL emission must be from InN quantum dots. (7) For wurtzite structure, in both cases of quantum dot and pure alloy, the PL polarization should be in the xy directions.

ACKNOWLEDGMENTS

I would like to thank Drs. W. Walukiewicz and J. Ager for interesting discussions. I would also like to thank Dr. A. Canning for a critical reading of the manuscript. This work was supported by the Director, Office of Science, Division of Mathematical, Information, and Computational Science of the U.S. Department of Energy under Contract number DE-AC03-76SF00098. This research used resources of the National Energy Research Scientific Computing Center, which is supported by the Office of Science of the U.S. Department of Energy.

REFERENCES

[1] S. Nakamura, J. Vac. Sci. Technol. A **13**, 705 (1995).

[2] S. Nakamura, M. Senoh, S. Nagahama, N. Iwasa, T. Yamada, T. Matsushita, H. Kiyoku, and Y. Sugimoto, Jpn. J. Appl. Phys. **35**, L74 (1996)

[3] S. Nakamura, Semicond. Sci. Technol. **14**, R27 (1999).

[4] S. Nakamura, Science **281**, 956 (1998).

[5] S. Chichibu, T. Azuhata, T. Sota, and S. Nakamura, Appl. Phys. Lett. **70**, 2822 (1997).

[6] N.A. El-Masry, E.L. Piner, S.X. Liu, S.M. Bedair, Appl. Phys. Lett. **72**, 40 (1998).

[7] M.D. McCluskey, L.T. Romano, B.S. Krusor, D.P. Bour, N.M. Johnson, and S. Brennan, Appl. PHys. Lett. **72**, 1730 (1998).

[8] K.P. O'Donnell, R.W. Martin, and P.G. Middleton, Phys. Rev. Lett. **82**, 237 (1999).

[9] C.K. Sun, S. Keller, G. Wang, M.S. Minski, J.E. Bowers, and S.P. DenBaars, Appl. Phys. Lett. **69**, 1936 (1996).

[10] W. Shan, J.J. Song, Z.C. Feng, M. Schurman, and R.A. Stall, Appl. Phys. Lett. **71**, 2433 (1997); W. Shan, B.D. Little, J.J. Song, Z.C. Feng, M. Schurman, and R.A. Stall, Appl. Phys. Lett. **69**, 3315 (1996).

[11] S. ChiChibu, K. Wada, S. Nakamura, Appl. Phys. Lett. **71**, 2346 (1997).

[12] D. Behr, J. Wagner, A. Ramakrishnan, H. Obloh, and K.H. Bachem, Appl. Phys. Lett. **73**, 241 (1998).

[13] V. Lemos, E. Silveira, J.R. Leite, A. Tabata, R. Trenin, L.M.R. Scolfaro, T. Frey, D.J. As, D. Schikora, and K. Lischka, Phys. Rev. Lett. **84**, 3666 (2000).

[14] Y. Narukawa, Y. Kawakami, M. Funato, S. Fujita, S. Fujita, and S. Nakamura, Appl. Phys. Lett. **70**, 981 (1997).

[15] I-hsiu Ho and G.B. Stringfellow, Appl. Phys. Lett. **69**, 2701 (1996).

[16] S.B. Zhang and A. Zunger, Appl. Phys. Lett. **71**, 677 (1997).

[17] L. Bellaiche, Appl. Phys. Lett. **75**, 2578 (1999); A. Al-Yacoub and L. Bellaiche, Phys. Rev. B **62**, 10847 (2000).

[18] L. Bellaiche, T. Mattila, L.W. Wang, S.H. Wei, and A. Zunger, Appl. Phys. Lett. **74**, 1842 (1999).

[19] L.W. Wang and A. Zunger, J. Chem. Phys. **100**, 2394 (1994).

[20] A. Canning, L.W. Wang, A. Williamson, and A. Zunger, J. Comp. Phys. **100**, 29 (2000).

[21] Landolt and Borstein, *Numerical Data and Functional Relationships in Science and Technology, Vol.22, Subvol. a* (Springer-Verlag, Berlin, 1997).

[22] C. Pryor, J. Kim, L.W. Wang, A.J. Williamson, and A. Zunger, J. Appl. Phys. **83**, 2548 (1998).

[23] A.J. Williamson, A. Zunger, and A. Canning, Phys. Rev. B **57**, R4253 (1998).

[24] P.W. Anderson, Phys. Rev. **109**, 1492 (1958).

[25] I.M. Lifshits, Sov. Phys. JETP **17**, 1159 (1963).

[26] L.W. Wang, L. Bellaiche, S.H. Wei and A. Zunger, Phys. Rev. Lett. **80**, 4725 (1998).

[27] This is done following a model, where a ball with natural lattice $a_{all} = a_{InN}x' + a_{GaN}(1-x')$ is embedded in a media of natural lattice $a_{medium} = a_{InN}x + a_{GaN}(1-x)$. The relaxed ball will then have a lattice of $a_{eq} = (Ba_{ball} + Aa_{medium})/(B+A)$, where $B = (C_{11}^{ball} + 2C_{12}^{ball})/3$ and $A = (C_{11}^{medium} - C_{12}^{medium})2/3$, and the C's are the elastic constants of a cubic system. We have used the x averaged elastic constants of InN and GaN for both the ball and the media.

[28] V.I. Klimov, Ch.J. Schwarz, D.W. McBranch, C.A. Leatherdale, and M.G. Bawendi, Phys.

Rev. B **60**, R2177 (1999).

[29] C.I. Harris and B. Monemar, Appl. Phys. Lett. **67**, 840 (1995).

[30] E.F. Schubert and W.T. Tsang, Phys. Rev. B **34**, 2991 (1986).

[31] E.F. Schubert, E.O. Gobel, Y. Horikoshi, K. Ploog, and H.J. Queisser, Phy. Rev. B **30**, 813 (1984).

[32] W. Shan, W. Walukiewicz, E.E. Haller, B.D. Little, J.J. Song, M.D. McCluskey, N.M. Johnson, Z.C. Feng, M. Schurman, and R.A. Stall, J. Appl. Phys. **84**, 4452 (1998).

[33] V.I. Litvinov, Appl. Phys. Lett. **77**, 2210 (2000).

[34] A. Tabata, J.R. Leite, A.P. Lima, E. Silveira, V. Lemos, T. Frey, D.J. As, D. Schikora, and K. Lischka, Appl. Phys. Lett. **75**, 1095 (1999).

[35] L.W. Wang, J. Kim, and A. Zunger, Phys. Rev. B **59**, 5678 (1999).

FIGURES

FIG. 1. Wavefunction squares of valence band maximum (VBM) and conduction band minimum (CBM) of InN quantum dots embedded in GaN matrix. For the three small dots $N_{In} = 1, 13$, and 43, the supercell box is $8a \times 8a \times 8a$, where a is the lattice constant, while a $16a \times 16a \times 16a$ supercell is used for the three larger quantum dots. For $N_{In} = 1, 13$ and 43, their CBM's are not bound, and not shown here.

FIG. 2. The CBM and VBM energies for the six quantum dots shown in Fig.1. For the three small dots, their CBM's are not bound. Thus we have used the bulk GaN CBM energy to represent their CBM energies.

FIG. 3. The VBM wavefunction square in a pure $In_{0.2}Ga_{0.8}N$ alloy. The supercell box is $16a \times 16a \times 16a$, where a is the lattice constant.

FIG. 4. The CBM and VBM energies of $In_{0.2}Ga_{0.8}N$ as functions of the number of In atoms in a 512 atom supercell. Each diamond symbol represents one alloy configuration, and there are 40 configurations in the plot.

FIG. 5. The calculated PL line width (a), average VBM energy (b), PL energy (c) and In percentage in the VBM wavefunction as functions of the In composition x in a $In_xGa_{1-x}N$ alloy. The experimental result in (c) is a linear fit to the experimental data in Ref. 32.

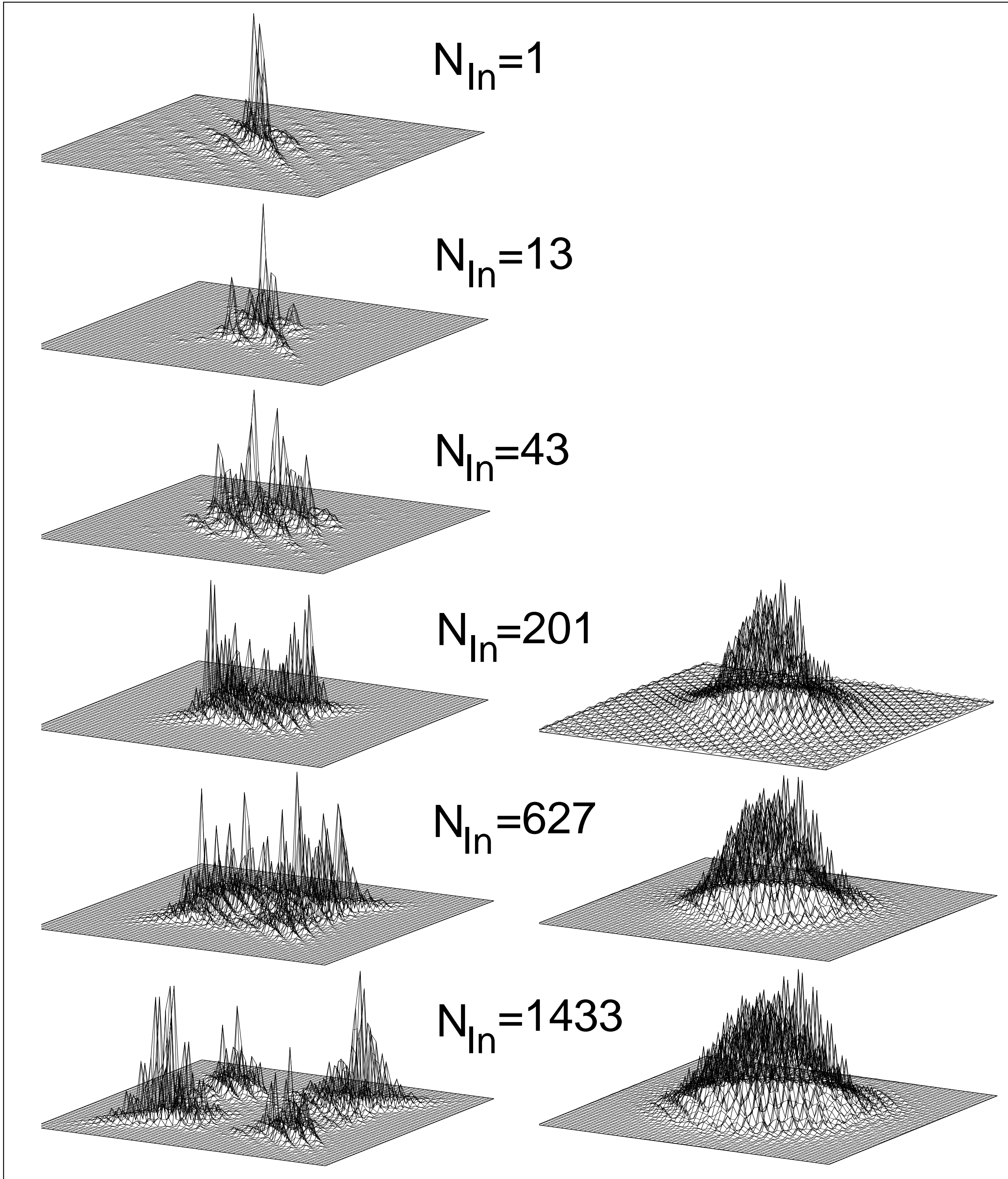

Fig.1, Wang

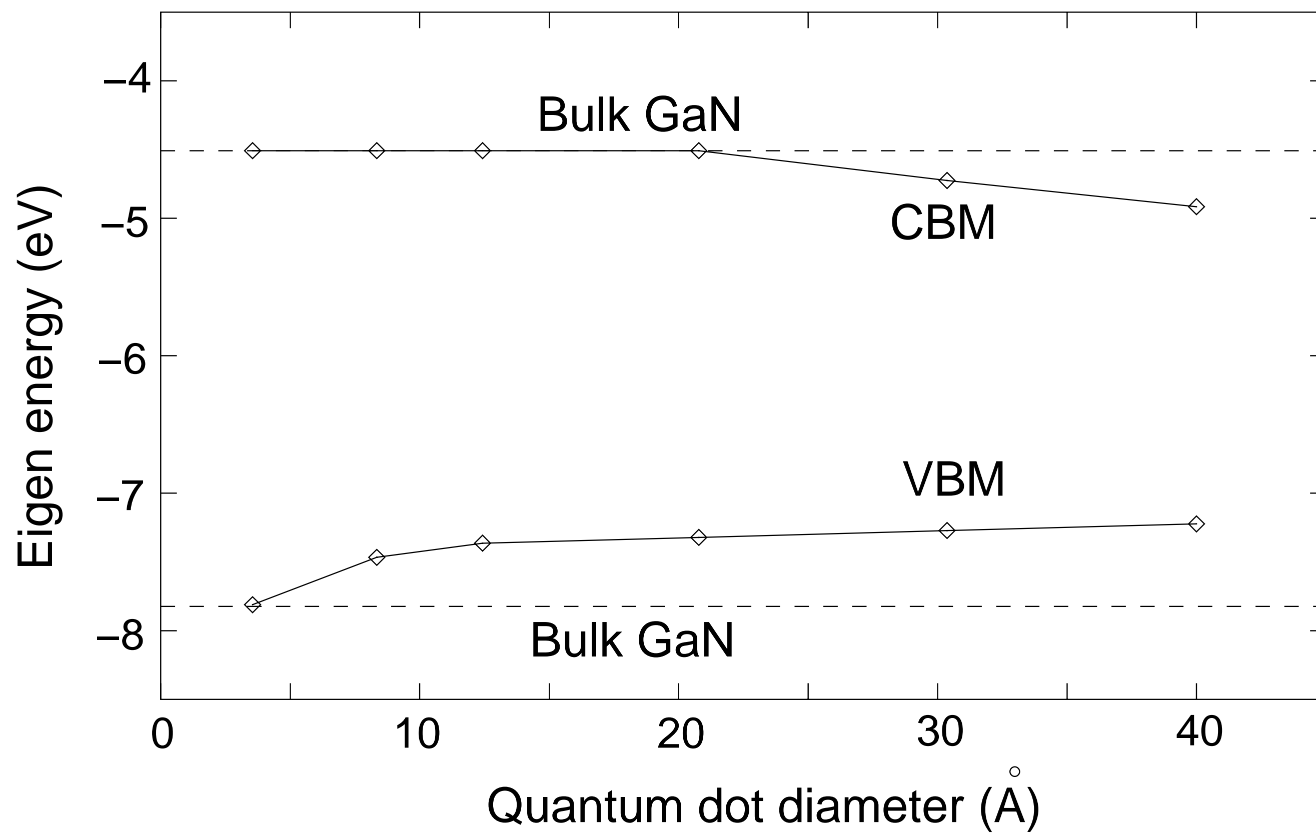

Fig.2, Wang

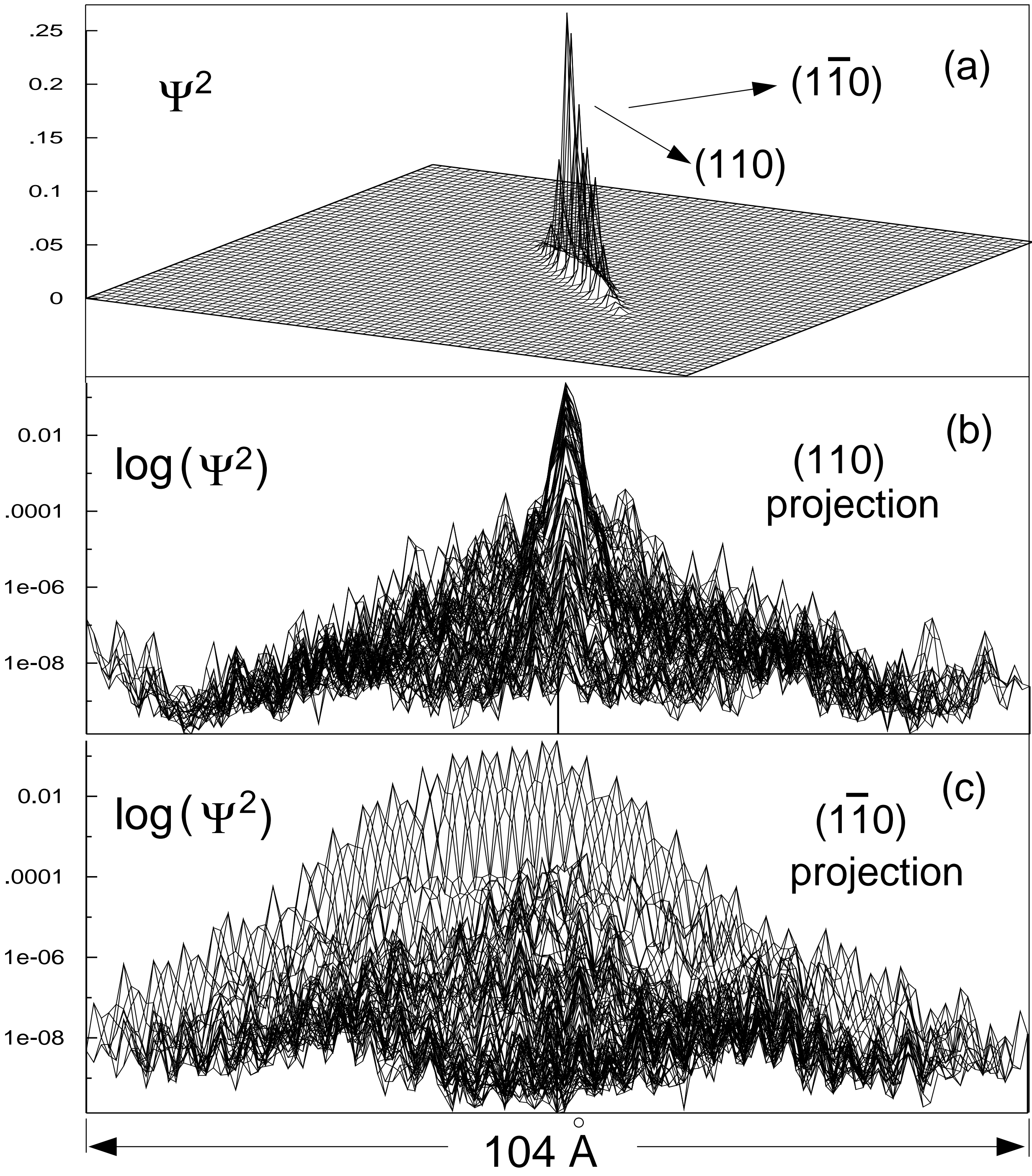

Fig.3, Wang

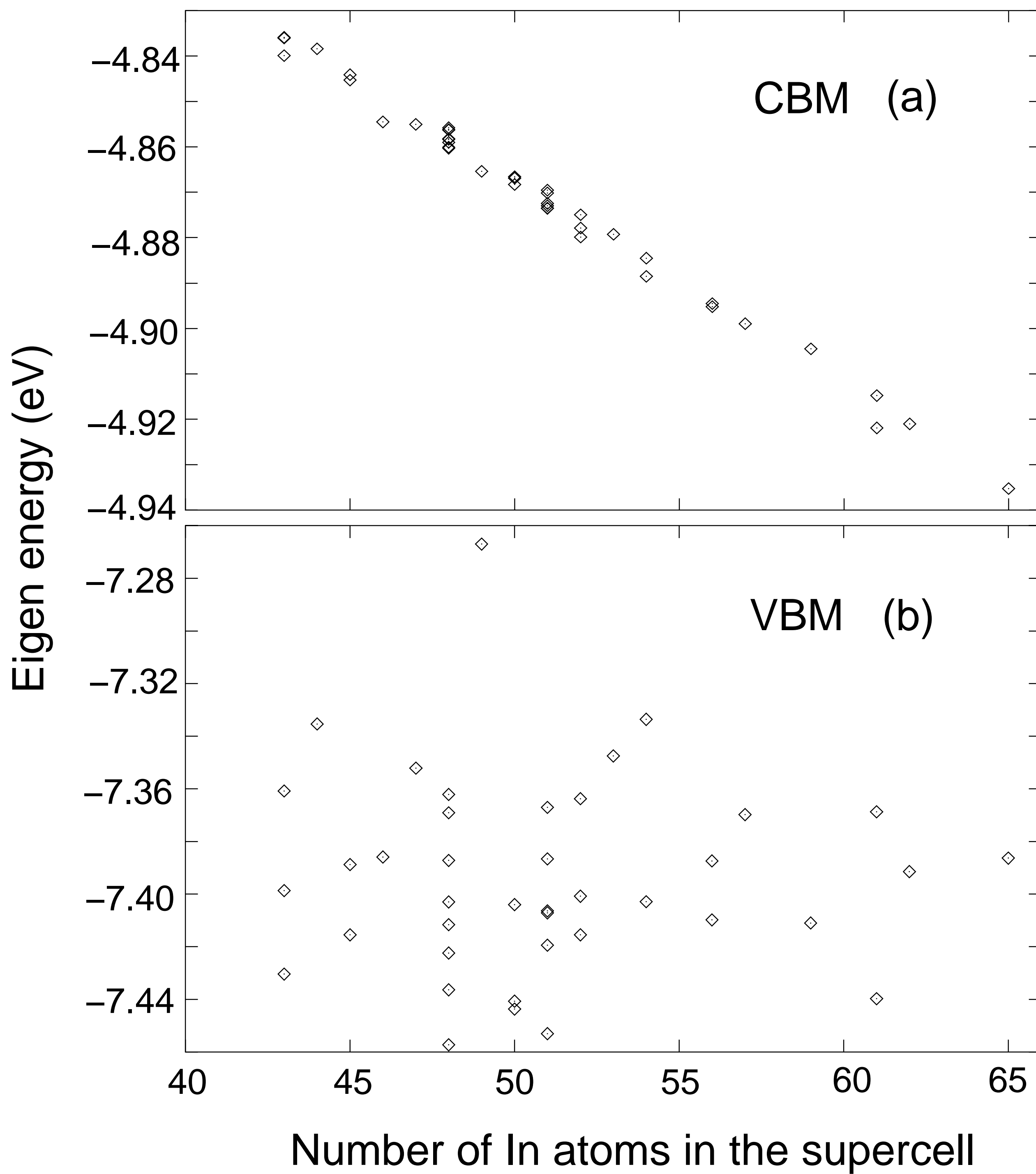

Fig.4, Wang

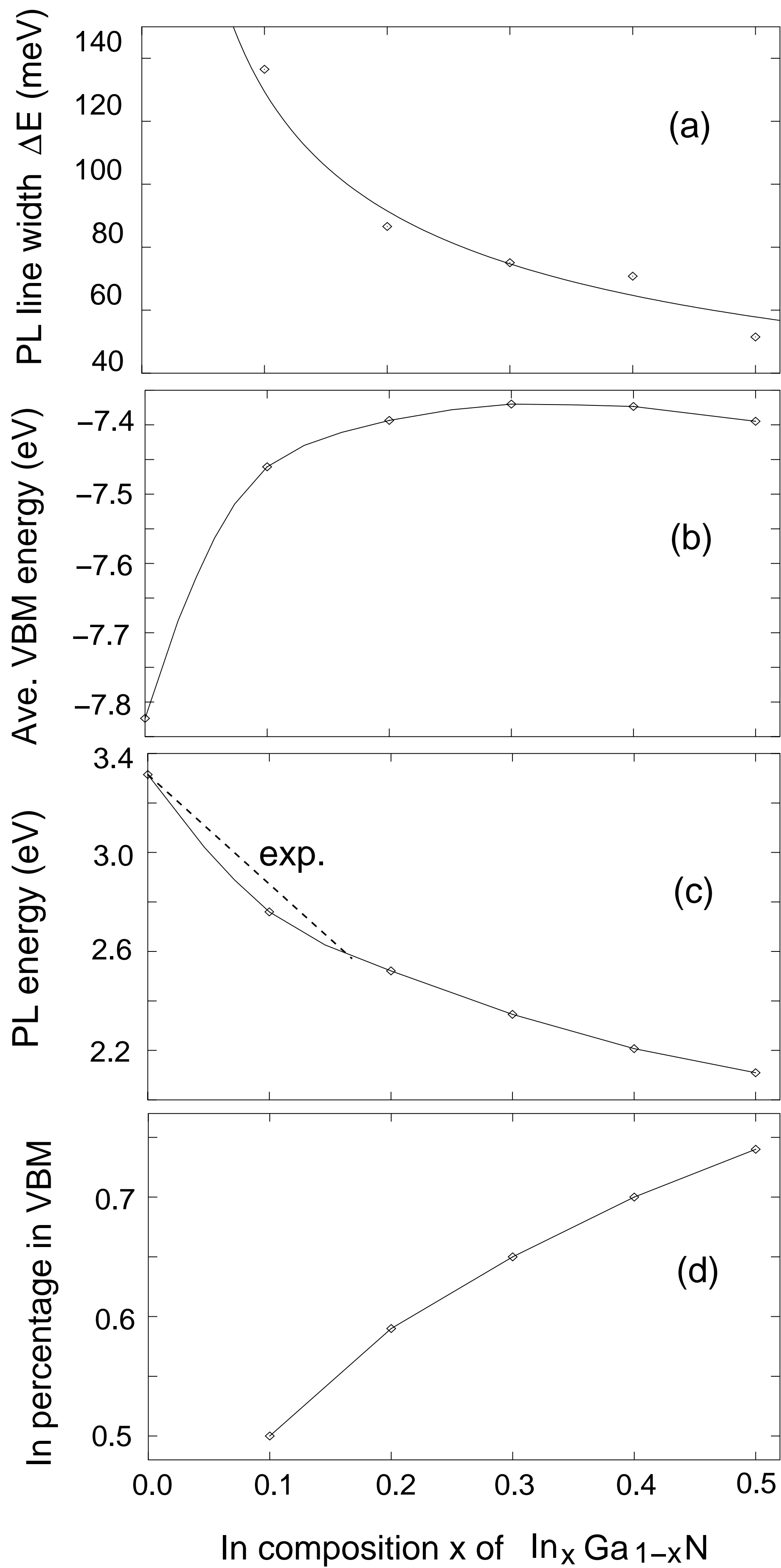

Fig.5, Wang